*International Journal of Latest Engineering and Management Research (IJLEMR)*
*ISSN: 2455-4847*
*www.ijlemr.com || Volume 06 - Issue 07 || July 2021 || PP. 19-32*

# Numerical studies for rectangular RC beams under shear forces

Maicon de Freitas Arcine[1], Nara Villanova Menon[2]
*[1](Master's Degree student/State University of Maringá, Brazil)*
*[2](Associate Professor, Department of Civil Engineering/State University of Maringá, Brazil)*

**Abstract:** Shearing forces affects a structure considerably resulting in a brittle collapse. This issue has been studied by many authors. However, many doubts still remain about such an effort. The objective of the present work was to calibrate numerical models in order to identify the main parameters that control the structural behavior of RC beams subjected to shear forces. For this, a bi-supported structure with and without stirrups was used. The software used was ABAQUS and the calibration consisted of varying the mesh size, the viscosity and the dilation angle in CDP model. The results were satisfactory in terms of cracking, load capacity, and final displacement. The parameter that most affected the results was viscosity. For the beam without stirrups, the diagonal shearing crack was more concentrated.

**Keywords:** ABAQUS, calibration, CDP model, RC beam, shear.

## I. INTRODUCTION

Most of the structures in civil engineering are built withy reinforced concrete (steel and concrete). According to the journal Concreto e Construções, of 2009 [1], concrete is the most used construction material in Brazil and in the world. Data from the Federación Iberoamericana de Hormigón Premezclado (FIHP) from 2009 [1] show that about 1.9 tons of concrete are consumed per inhabitant per year, a figure only lower than water consumption. In the Brazilian territory, consumption is around 30 million cubic meters. It is noted worldwide that concrete structures are present throughout the human routine, providing safety and comfort.

However, several factors may affect the performance of a structural element, such as load increments; damage to structural parts (aging, fires, framework corrosion, vehicle impact, etc.); modification of the structural system; design, calculation, and construction errors. If poorly evaluated, these occurrences can cause structural damage and, consequently, breakage of the structure.

Shear failures in reinforced concrete beams, both with and without stirrups, usually develop suddenly and without notice. These failure modes are undesirable and jeopardize a structural project, to which, preferably, the collapse must be preceded by warning signals, such as those before a ductile failure by bending (visible fissures and large vertical displacements) [2]. The study of shear failures has proved to be highly complex, as demonstrated by the large number of researchers on the subject [3–6], most of them being focused on experimental evaluations.

The application of MEF (Finite Element Method) enables the calibration of a numerical model with experimental results and its extension to evaluate other situations. Therefore, the use of numerical analysis to supplement an experimental study about shear in reinforced concrete beams will help future researchers to understand the structural behavior. It will also contribute to save time and money with modeling. An example of a computational program capable of solving problems related to this subject is the software ABAQUS 6.12[7], based on the Finite Element Method (FEM).

The computational modeling of reinforced concrete is quite extensive. Based on experimental evidences, simulations with this Software show the tensions and deformations generated in rectangular reinforced concrete beams [8]. Studies investigating the damage in the material can be detailed, obtaining patterns of cracking and damage detection in their early stages [5,9–13]. Other studies aim at increasing the resistant capacity of a reinforced beam to the bending and shearing of these structures [14,15]. Within this context, the purpose of this work is to delineate, by means of numerical simulations, the failures and structural behavior of rectangular beams in reinforced concrete subjected to shearing.

## II. MATERIALS AND METHODS

### 2.1 Concrete Damage Plasticity (CDP)

The multi-axial model called Concrete Damage Plasticity (CDP), proposed by Lubliner et al. [16]and developed by Lee and Fenves [17], is described as a model in the form of effective tension. According to Lubliner et al. [16], any plasticity model for concrete must involve four basic assumptions: Laws of damage evolution, Initial plasticizing surface (Yield criterion), Hardening/Softening law, and Flow rule.

The CDP offers the ability of progressive modeling damage to a material. This damage is described by the variable "d" and its value is initially zero when the material is fully integrated and 1 when fully damaged

($0 \leq d \leq 1$). The damage factors $dc$ and $dt$ represent the rate of degradation of concrete rigidity caused by material damage during compression (crushing) and traction (cracking), respectively, under uniaxial stress (Fig. 1). Demin and Fukang [18]stressed that the CDP model in the ABAQUS[7] program is considered adequate for quasi-fragile materials, in this case, concrete.

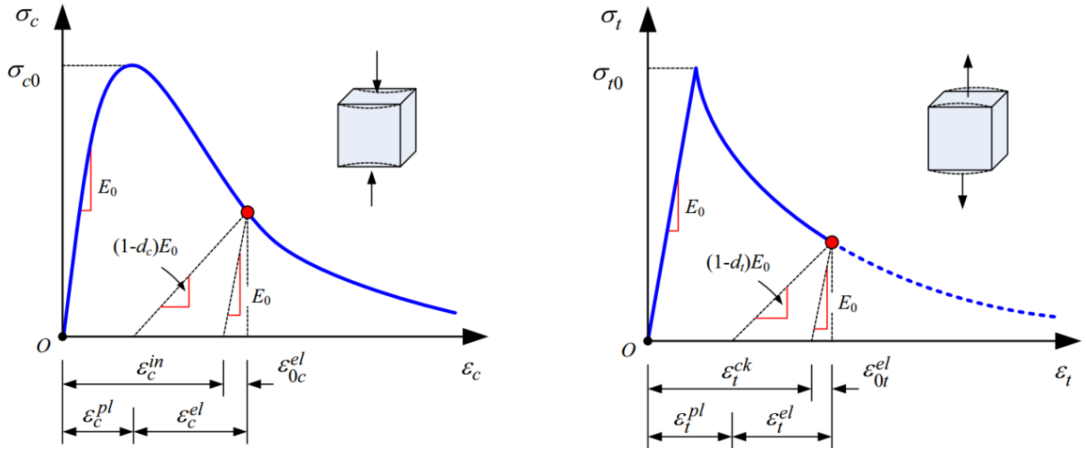


**Fig. 1**. Concrete CDP Tension x Strain for uniaxial tension of compression (a) and traction (b)[19].

The concrete response in the uniaxial compression tension x strain diagram (Fig. 1 (a)) is linear up to the yield stress value ($\sigma_{c0}$). From this stress, the plastic regime is initiated, resulting in an increasing stress until the ultimate stress is reached ($\sigma_{cu}$). Consequently, there is a decrease in the elasticity modulus. As a result, the tension decreases and the strain increases. Regarding the concrete response under traction (Fig. 1 (b)), a linear elastic relation is followed until the failure tension value is reached ($\sigma_{t0}$), in which, from this point on, micro-cracks appear in the concrete. At values higher than this stress, the graph also shows a decrease in the elasticity modulus in the curve, which induces local deformation in the concrete structure. Consequently, the tension decreases and the strain increases. In the diagrams there is a change of value in the modulus of elasticity in the plastic regime, this value being called the damaged (or effective) elasticity modulus, ($\bar{E}$), being defined as:

$$\bar{E} = (1 - d).E_0 \quad (1)$$

Where $E_0$ is the initial elasticity modulus, elastic or undamaged. Equations 2 and 3 present the function of the stress state as a function of the initial elasticity, the strain tensors, and the damage during compression ($dc$) and traction ($dt$):

$$\sigma_t = (1 - d_t)E_0(\varepsilon - \varepsilon^{pl});\ \bar{\sigma}_t = E_0(\varepsilon_t - \varepsilon_t^{pl}) \quad (2)$$

$$\sigma_c = (1 - d_c)E_0(\varepsilon - \varepsilon^{pl});\ \bar{\sigma}_c = E_0(\varepsilon_c - \varepsilon_c^{pl}) \quad (3)$$

Where $\sigma_t$ and $\sigma_c$ are effective tension and compression values, respectively, $\varepsilon$is deformation and $\varepsilon^{pl}$ is plastic deformation, both may refer to traction ($\varepsilon_t$ and $\varepsilon_t^{pl}$) or compression ($\varepsilon_c$ and $\varepsilon_c^{pl}$).

According to Chi et al.[19], this yield surface defines the critical stress state, beyond which the plastic deformation begins. The yield criteria that are most used for the materials are those of Mohr–Coulomb and Drucker– Prager and may be written in terms of effective stresses, such as:

$$F(\bar{\sigma}) = \frac{1}{1-\alpha}(\bar{q} - 3\alpha\bar{p} + \beta_1(\varepsilon^{pl})\langle\bar{\sigma}_{máx}\rangle - \gamma_a\langle\bar{\sigma}_{máx}\rangle) - \bar{\sigma}_c(\varepsilon_c^{pl}) = 0 \quad (4)$$

This function uses two stress invariants of the stress tensor, which are the effective hydrostatic stress $\bar{p}$hydrostatic $\bar{q}$. The constants $\alpha$, $\beta$, and $\gamma$ are dimensionless, $\bar{\sigma}_{máx}$ is the maximum algebraic value of the major effective stresses and $\langle . \rangle$ is the Macauley operator defined as $\langle x \rangle = (|x| + x)/2$.

According to Lubliner et al.[16], for granular materials, such as concrete, due to changes in the plastic strains, this material may exhibit significant volume changes. For this purpose, the CDP model assumes a function for the plastic potential with a non-associative rule. The function adopted for the plastic potential Q for this model is based on the hyperbolic function of Drucker-Prager, obtained generically by:

$$Q = \sqrt{(mf_t tan\psi)^2 + \bar{q}^2} - \bar{p}tan\psi \quad (5)$$

Where $\psi$ is the angle of dilation measured at the plane $p - q$, $f_t$ is the uniaxial failure tensile stress and $m$ is a parameter identified as eccentricity. These three parameters indicate the hyperbolic function of Drucker-Prager's potential flow [20].

### 2.2 Constitutive model for steel

In general engineering applications, usually a elastic-perfectly plastic behavior of steel components is adopted, identical in its tension and strain, being also used by Obaidat et al. [21]. The criteria of Von Mises are generally adopted for this model. The parameters that define such model are: modulus of elasticity$E_s$, yield stress $f_y$, and Poisson coefficient $\upsilon$.

### 2.3 Bond-slip model

In a reinforced concrete beam, the relative displacement between a steel bar and the concrete is controlled by the behavior of the bond between these materials. This relationship can result in more or less ductile reinforced concrete beam [22].

Generally, in numerical simulations, the perfect bond between steel and concrete is adopted (embedded bars), which leaves a stiffer reinforced concrete beam. However, the effects of sliding may be considered using interface elements that connect the degrees of freedom of the bars and the concrete mesh. Another method is to modify the properties of the steel bars (yield stress and equivalent modulus of elasticity) in order to model the sliding effects (Fig. 2) [23]. In this sense, the second assumption was addressed in this work due to the simplicity of the method and its effectiveness [22].

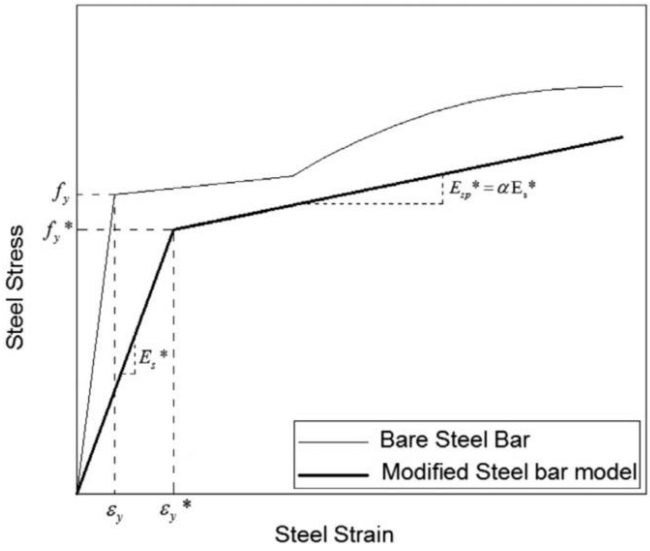


**Fig. 2.**Stress x modified strain ratio for steel bars inserted in reinforced concrete girders[22].

As previously observed, the response of steel to traction has a bilinear behavior with both a yield and a failure stress. Belarbi and Hsu [24]described a relation from experimental data to which the real elasticity limit of the steel bar inserted in the concrete can be obtained as:

$$f_y^* = f_y\left(0.93 - \frac{2}{\rho}\left(\frac{f_t}{f_y}\right)^{1.5}\right) \quad (6)$$

Where $f_y$ is the steel yield stress (MPa), $f_y^*$ is the reduced or equivalent yield stress (MPa), $\rho$ is the longitudinal steel rate, and $f_t$ is the concrete tensile resistance (MPa). In studies, Kwak and Kim [25]used the bilinear relation of tension x strain and modified this constitutive law, reducing its rigidity. Dehestani and Mousavi [22]proposed a similar model, although for the calculation of the equivalent modulus of elasticity, they also suggested reducing the yield stress as before. The following equation indicates the calculation of the new stiffness:

$$E_s^* = f_y^*/(\varepsilon_s + \delta_e/l) \quad (7)$$

In Equation 7, we must determine the maximum value of bar slipping (sliding) in mm, defined by $\delta_e$. The expression of Wu and Zhao [26]was used to estimate such factor. The parameter $l$ represents the transmission length between the bar and the concrete in millimeters (mm), calculated according to Kwak and Kim [25]. Finally, we have $\varepsilon_s$, which means the deformation corresponding to $f_y^*(f_y^*/E_s^*)$ (mm/mm).

### 2.4 Characteristics of the simulated beams

The studied beam was tested by Menon [27], breaking through the crack at the shear span, called shear critical diagonal, after the development of small bending fissures. This diagonal collapse at 77,71 kN and the maximum displacement found under the applied load was approximately 1,11cm (111 mm).The structure has a

120 x 250 mm cross-section with a total length of 2500 mm. Both the compression and traction longitudinal bars were composed of four CA-50 steel bars of 16mm each. The stirrups were CA-60 steel with 4,2 mm wide. The details of the beam are show in Fig. 3.

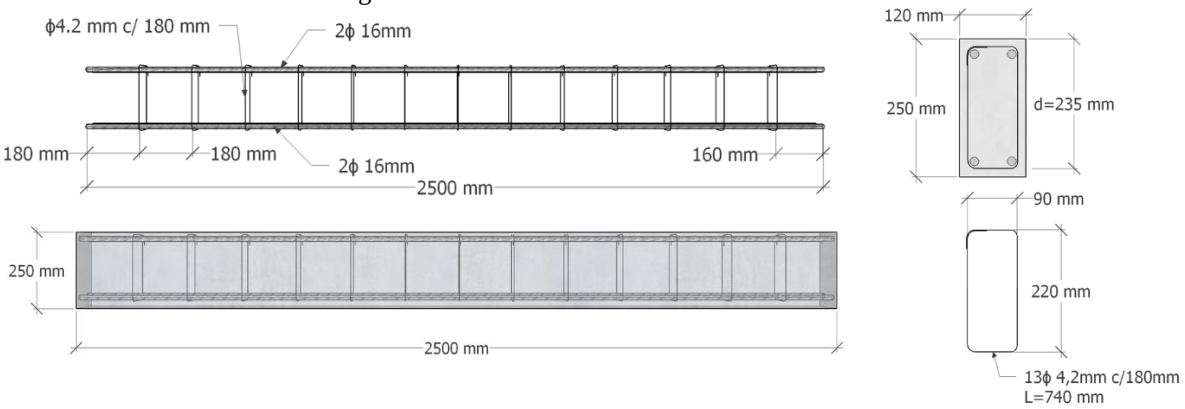


**Fig. 3**. Beam detailing, adopted[27]**.**

The concrete used in the experiment was dosed in central, with a specified $f_{ck}$ of 30 MPa. The concrete resistance obtained experimentally was 31,20 MPa at 28 days. The steels used in the longitudinal and transversal framework of the concrete beam were tested for traction and yield and rupture stresses, with the results shown in

Table **1**.

**Table 1**. Steel properties[27]**.**

| Steel | Specimen | Diameter (mm) | Yield Stress (MPa) | Ultimate stress (MPa) |
|---|---|---|---|---|
| CA-60 | 1 | 4,20 | - | 790,96 |
| CA-60 | 2 | 4,20 | - | 805,61 |
| CA-50 | 1 | 16,00 | 591,74 | 730,97 |
| CA-50 | 2 | 16,00 | 606,66 | 740,95 |

The beams were arranged on second and first type supports and then received a load $P$ through a hydraulic jack, as shown in Fig. 4. The value of the shear span ratio $(a/d)$ was 2,68.

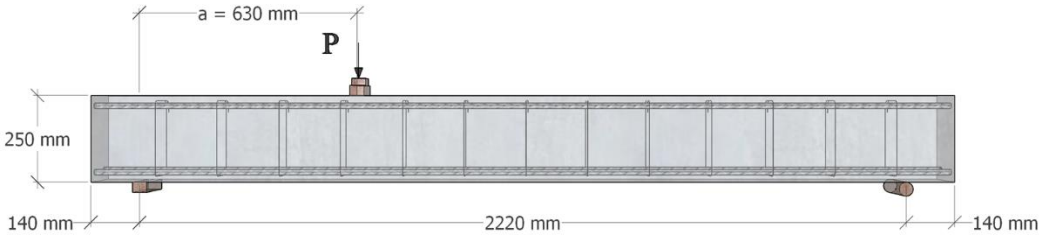


**Fig. 4.**Boundary conditions**,** adopted[27]**.**

## 2.5 Numerical analysis

The applied load was in the form of displacement over a rigid element, as well as the supports. The modeling proceeded with the application of this characteristic on the beam, since it was symmetric one plane. The element used as concrete in the simulation was the C3D8R and the model was the CDP. The simulation strategy adopted was that of Newton - Raphson. These characteristics are best represented in Fig. 5.

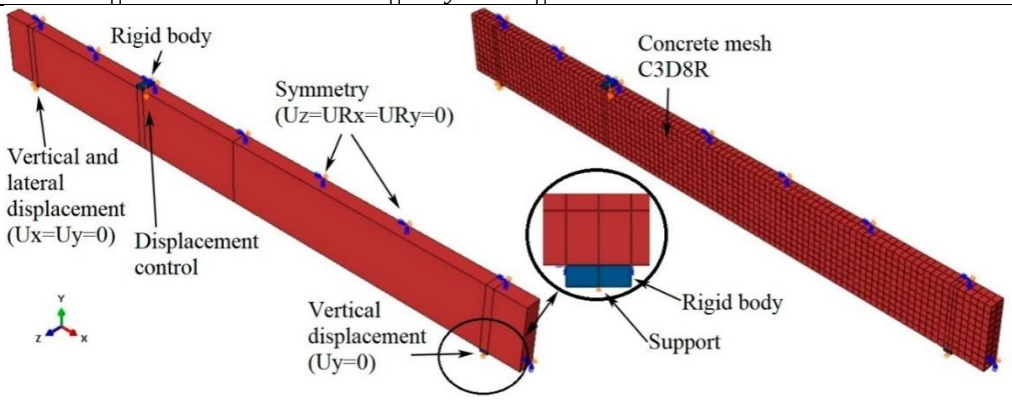


**Fig. 5.** Boundary conditions (a) and discretization of the elements (b).

The calibration was based on the variation of the finite element in 50 mm (562 elements), 40 mm (804 elements), 30 mm (1404 elements), and 25 mm (2072 elements). The dilation angles tested were 32°, 35°, 38°, and 40°. The viscosity was also tested and varied between $10^{-5}$, $10^{-4}$, $10^{-3}$ and $10^{-2}$. The other CDP parameters were based on the current literature (Table 2).

**Table 2.** CDP parameters according to the current literature.

| Reference | $f_c'$ (MPa) | Concrete structure | Ψ | $m$ | $\frac{f_{bc}}{f_c}$ | $K_c$ | $\mu$ |
|---|---|---|---|---|---|---|---|
| Genikomsou and Polak [28] | 33 – 46 | Slab/Column | 40° | 0,1 | 1,16 | 0,667 | $10^{-5}$ |
| Najafgholipour *et al.*[29] | 41– 46 | Beam/Column | 35° | 0,1 | 1,16 | 0,667 | $8.\ 10^{-3}$ |
| Demin and Fukang [18] | 26,8 | Beam | 30° | 0,1 | 1,16 | 0,667 | $10^{-4}$ |
| Al-Osta *et al.*[30] | 54 | Beam | 36° | 0,1 | 1,16 | 0,667 | 0 |
| Li, Hao and Bi[31] | 48,7 – 57,3 | Column | 30° | 0,1 | 1,16 | 0,667 | $10^{-4}$ |
| Behnam, Kuang and Samali [32] | 34,7 – 36,1 | Beam/Column | 40° | 0,1 | 1,16 | 0,667 | $10^{-5}$ |
| Gao *et al.*[34] | 50 | Beam | 35° | 0,1 | 1,16 | 0,667 | - |
| Jumaa and Yousif [13] | 43,2 – 73,4 | Beam | 30° | 0,1 | 1,16 | 0,667 | 0 |
| Dabiri *et al.* [35] | 18,4 – 19,2 | Beam/Column | 40° | 0,1 | 1,16 | 0,667 | $10^{-5}$ |

The constitutive curves of the concrete under compression and traction were obtained according to Carreira and Chu [36]and Hordjik [37], respectively. The traction resistance of the concrete was estimated using the equation of Genikomsou and Polak [28], expressed by $f_t = 0{,}33\sqrt{f_{ck}}$. The elasticity modulus was estimated using the American standard ACI 318 [38]and the peak compression straining was assessed according to Carreira and Chu [36]. The Poisson coefficient for all tests was 0,2 for concrete and 0,3 for steel. The evolution of the damage was calculated according to Birtel and Mark [39]. The parameters $b_c$ and $b_t$ were 0,6 and 0,9, respectively.

Regarding the steel used in the reinforcement, the model used was the perfect elastoplastic (Von mises criteria). The interaction of concrete with steel was considered perfect, i.e., with a portion (steel) embedded in the concrete (Embedded region). The bond-slip model was adopted to simulate the sliding effect between concrete and steel and obtain more realistic results. Then, the beam was tested without this model and the results compared. The meshes adopted for the longitudinal bars were 10 mm (250 elements) and 3 mm (103 elements) for the stirrups. The element used was T3D2 for both bars.

After calibration of the structure, practically all the transversal reinforcement was removed from the beam, leaving only 3 stirrups, as in Fig. 6, and then once more simulated. The structure with stirrups was named V0-E and the one without stirrups V1-S.

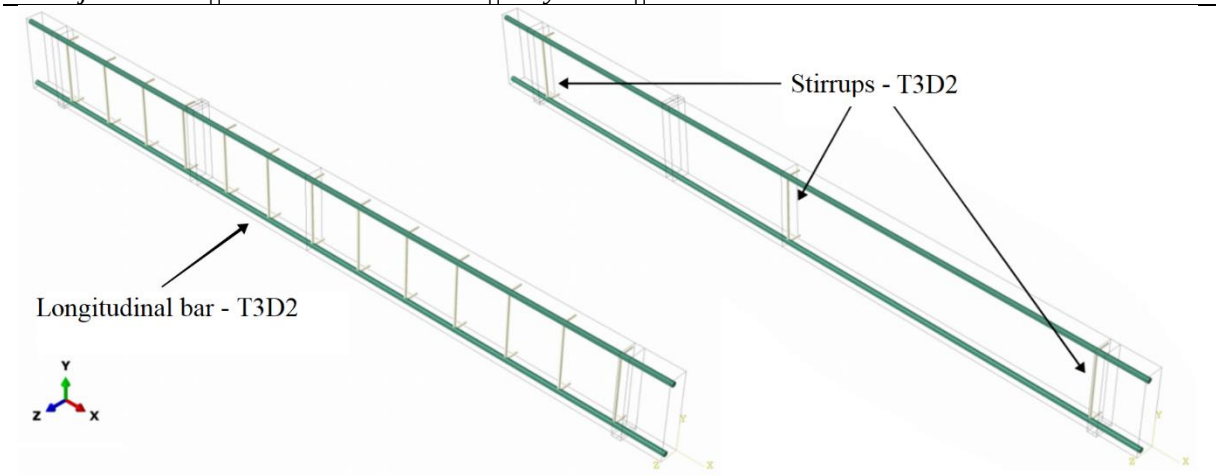


(a) (b)

**Fig. 6.** RC beam (V0-E) with stirrups (a) and RC beam (V1-S) without stirrups (b).

## III. RESULTS AND DISCUSSIONS

The computer used in the analysis has 8GB (RAM), a Core processor (TM) i5-7300HQ, 2.50 GHz CPU with 4 cores and a GeForce GTX 1050 video board. Table 3 presents the different values of each of the parameters, as well as the results and processing time of each simulation. All the displacements were assessed at the middle of the span.

**Table 3.** Results of the calibration of the V0-E beam.

| Parameter | Values | $P_{num}$ (kN) | Constants parameters | Displacement (mm) | $\frac{P_{exp}}{P_{num}}$ | Processing |
|---|---|---|---|---|---|---|
| Mesh size (mm) | 50 | 79,51 | $\mu = 10^{-4}$ $\psi = 38°$ $f_{bc}/f_c = 1{,}16$ $m = 0{,}1$ $K_c = 0{,}667$ | 9,42 | 0,98 | 00:05 h |
| | 40 | 79,17 | | 8,60 | 0,98 | 00:09 h |
| | 30 | 82,48 | | 10,94 | 0,94 | 00:19 h |
| | **25** | **79,55** | | **9,12** | **0,98** | **00:22 h** |
| Viscosity ($\mu$) | $10^{-5}$ | 76,96 | Mesh = 25mm $\psi = 38°$ $f_{bc}/f_c = 1{,}16$ $m = 0{,}1$ $K_c = 0{,}667$ | 8,08 | 1,00 | 00:46 h |
| | **$10^{-4}$** | **79,55** | | **9,12** | **0,98** | **00:22 h** |
| | $10^{-3}$ | 81,32 | | 11,33 | 0,96 | 00:09 h |
| | $10^{-2}$ | 118,00 | | 11,02 | 0,66 | 00:03 h |
| Dilatation angle | 32° | 67,38 | Mesh = 25mm $\mu = 10^{-4}$ $f_{bc}/f_c = 1{,}16$ $m = 0{,}1$ $K_c = 0{,}667$ | 7,00 | 1,15 | 00:36 h |
| | 35° | 68,00 | | 8,32 | 1,14 | 00:31 h |
| | **35°** | **79,55** | | **9,12** | **0,98** | **00:22 h** |
| | 40° | 82,12 | | 10,11 | 0,95 | 00:16 h |

The experimental beam reached a maximum load of 77,7 kN with a displacement of approximately 9,10 mm. All models that varied the finite element mesh presented results similar to the experimental models, both in maximum loads and in behavior of the load x displacement curve [28,29]. According to Genikomsou and Polak[28], the small dependence on the mesh size is present in most plasticity models that consider the softening and straining phenomena in the constitutive equations. Among the ways to decrease the mesh size dependence are: introduction of the evolution of the crack opening in the softening part of the constitutive model and normalization of the viscosity parameter. Najafgholipour et al. [29] stated that, in fact, the size of the mesh does not affect considerably the general response of the numerical model. Regarding the experimental curves, the 25 mm mesh was the one closest to reality, as well as its displacement being practically the same as the experimental one (Fig. 7 (a)). As expected, as the mesh became less dense, the processing time decreased.

The viscosity parameter is a mathematical tool that reduces the sensitivity of the mesh to constituent models that present a softening behavior, as in the case with concrete. The higher the value of this parameter, the greater is the area of influence of the damage. Fig.7 (b) shows the comparison of the results with the variation of $\mu$ is show in Fig. 7 (b), demonstrating that the higher the viscosity, the shorter the simulation time. However, according to Dabiri et al. [35], the model tends to overestimate this value, resulting in an unreliable numerical model. The best results were around 0,0001, this value being used in the next simulations

The angle of dilation is related to the plastic potential function and describes the inclination angle of the plastic potential surface. For this reason, it is linked to plasticity and later rupture of the material. The evolution of the load x displacement curve with the variation of the dilation angle is show in Fig. 7 (c). Malm [40]observed that small values of this parameter (around 10°) leave the response of the concrete more fragile, while larger angles (above 40°) produce more ductile responses and higher peak loads, which was also found in this work. The observed values showed that, in this study, the value of the expansion angle that best represents the behavior of the experiment is 38°.

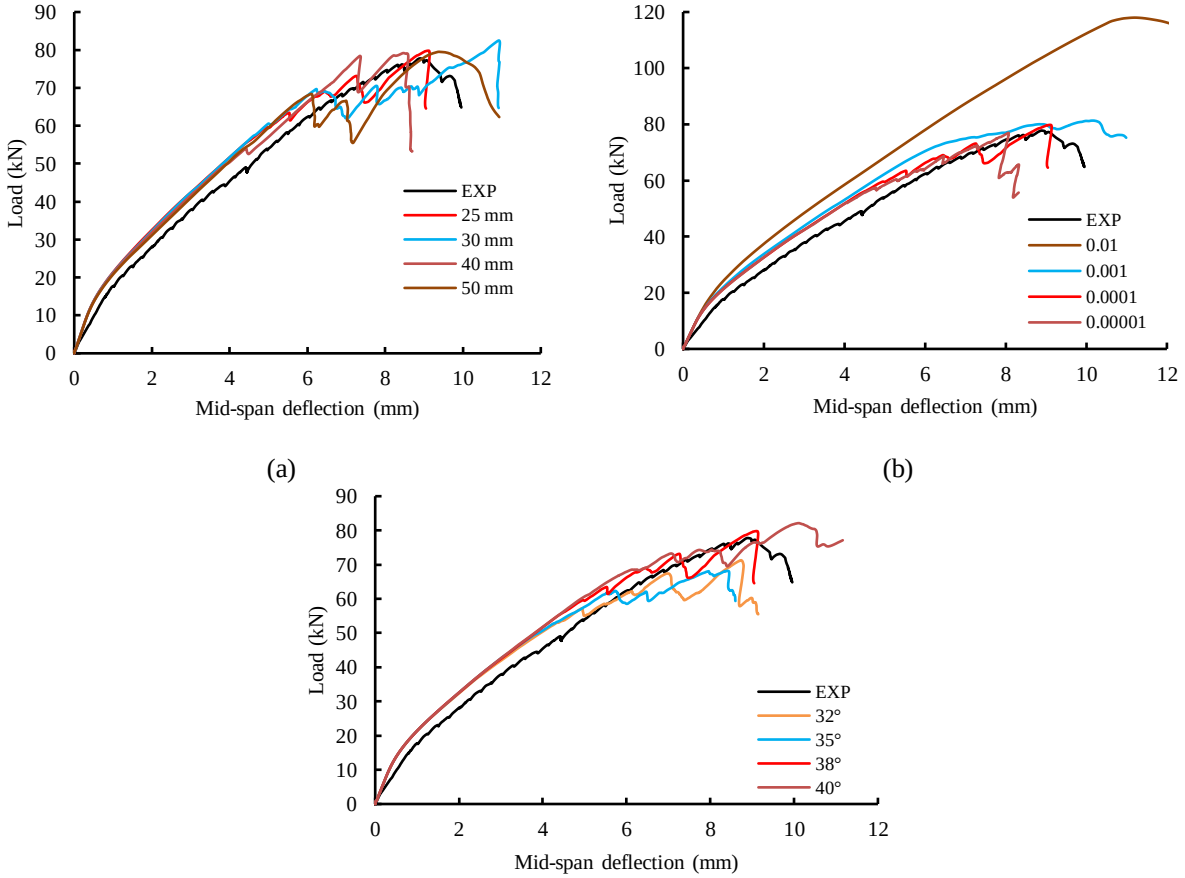


**Fig.7.** Simulations of the V0-E beam with variation of mesh size (a), viscosity (b) and dilation angle (c).

Therefore, with the results obtained, it was possible to construct a realistic load x numerical displacement graph. This curve is show in Fig. 8, together with the summary of the calibration in Table 4 and some important points for the concrete stress and crack analysis.

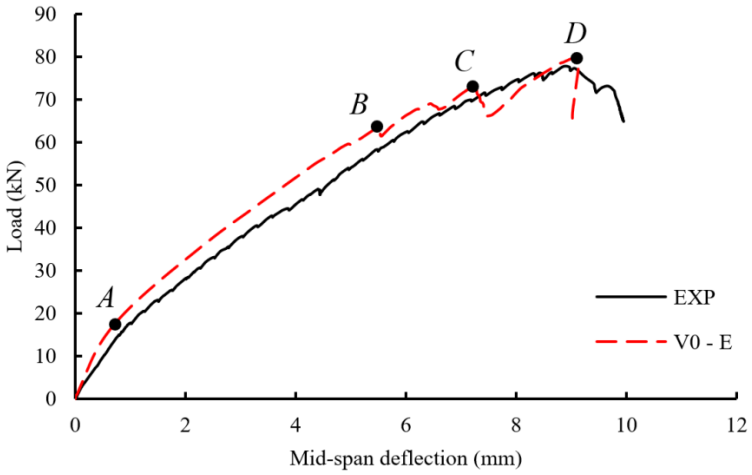


**Fig. 8.** Load x displacement graph at the middle span for the V0-E beam.

**Table 4.**Overview of the calibration of the V0-E beam.

| Beam | $P_{num}$ (kN) | Displacement (mm) | $\frac{P_{exp}}{P_{num}}$ | Mesh size (mm) | $f_{bc}/f_c$ | $m$ | $K_c$ | $\mu$ | $\psi$ |
|---|---|---|---|---|---|---|---|---|---|
| V0-E | 79,55 | 9,42 | 0,98 | 25 | 1,16 | 0,1 | 0,667 | 0,0001 | 38° |

With the adoption of the bond-slip model for steel, the global rigidity of the simulated structure approached the experimental one and it was possible to obtain good results, which was also observed by Jumaa and Yousif [13]. However, it is very difficult to achieve the exact behavior of the structure. According to Jumaa and Yousif [13], the microcracks produced by retraction of the concrete also decrease the rigidity of the experimental beams, and in numerical modeling, the materials were considered homogeneous, not being taking into account this factor. Table 5 shows the values that were used in the simulations.

**Table 5.** Variation of the parameters of longitudinal bars using the bond-slip model.

| $f_{cm}$ (MPa) | $E_s$ (GPa) | $E_s^*$ (GPa) | $f_y$ (MPa) | $f_y^*$ (MPa) | $l$ (mm) |
|---|---|---|---|---|---|
| 31,20 | 210,00 | 146,73 | 599,20 | 549,63 | 281,70 |

Fig.9 (a) shows the development of the cracks and Fig. 9 (b), the evolution of the traction damage in concrete. Observing both, from the beginning of loading to point A of Fig. 8, there was no substantial damage to concrete, recalling that the damage varies from 0 to 1, as well as the absence of considerable cracks. This stage is characterized as the beginning of the nonlinear behavior of the structure, as well as the experimental one.

The first bending cracks in the concrete begin to appear from point A to point B and, consequently, its change of rigidity due to the evolution of the damage. The evolution of the bending cracks in the left branch of the beam is highlighted. The formation of the main shear cracking begins at point C. At this stage, the experimental study reached the yield of the stirrups in the shear span. Since CA60 steel does not have an evident hardness, its respective value was not informed in the numerical simulation. When analyzing the results of the numerical study between stages C and D, the stress in the stirrups varied from 568MPa to 798MPa, respectively (Fig. 11). Since 798MPa is the rupture value for the stirrup, it is assumed that it reached the yield stress during this stage. Finally, point D is characterized by the system collapse, with the formation of the critical shear and other bending cracks.

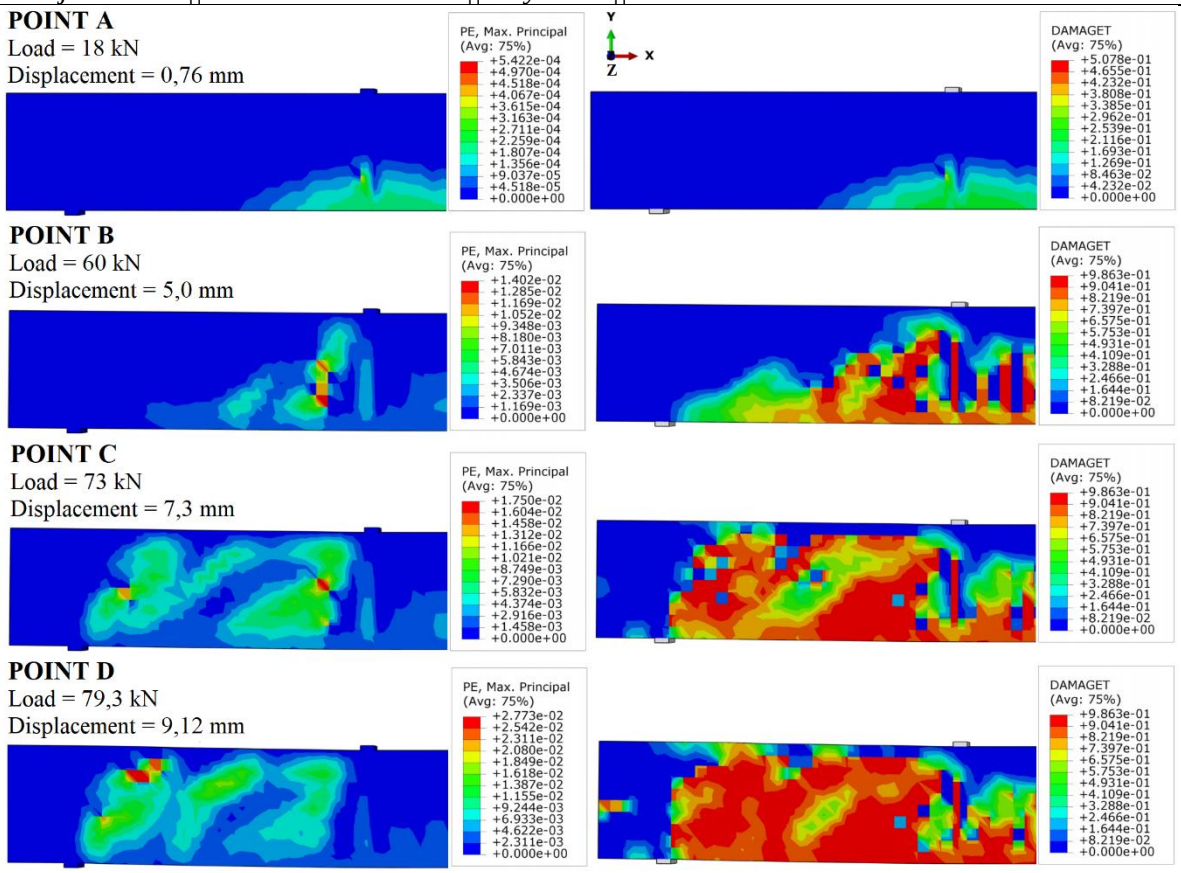


(a) (b)

**Fig.9.** Crack evolution (a) and traction damage (b) in the V0-E beam.

Fig. 10 presents a comparison of the V0-E beam cracking scenario with the experimental one, showing the formation of the main shear cracking at the critical diagonal, as well as the bending cracks in the concrete.

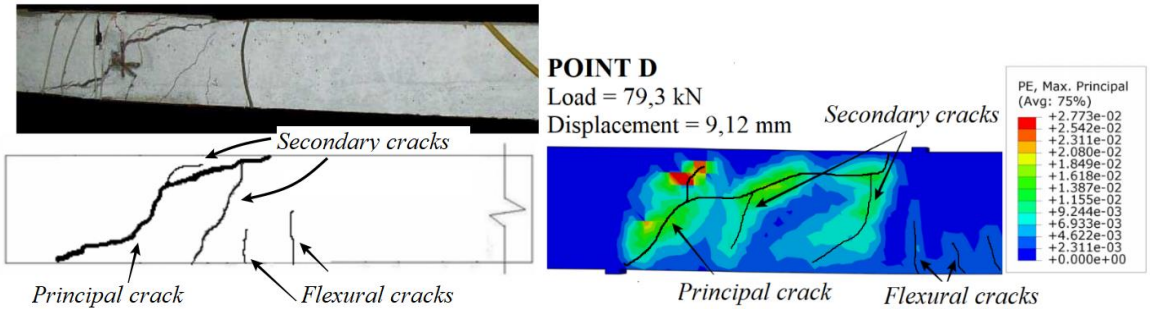


(a) (b)

**Fig. 10.**Comparison of the cracking scenario of the experimental beam (a) with the V0-E beam (b).

The evolution of Von Mises' tensions in the steel reinforcements were compared in Fig. 11. The steel of the longitudinal framework did not experience yield stress, presenting a maximum tension of 406,2 MPa. Regarding the stirrups highlighted at point D, they were the most requested, mainly from point C on, where the critical shear cracking begins to appear.

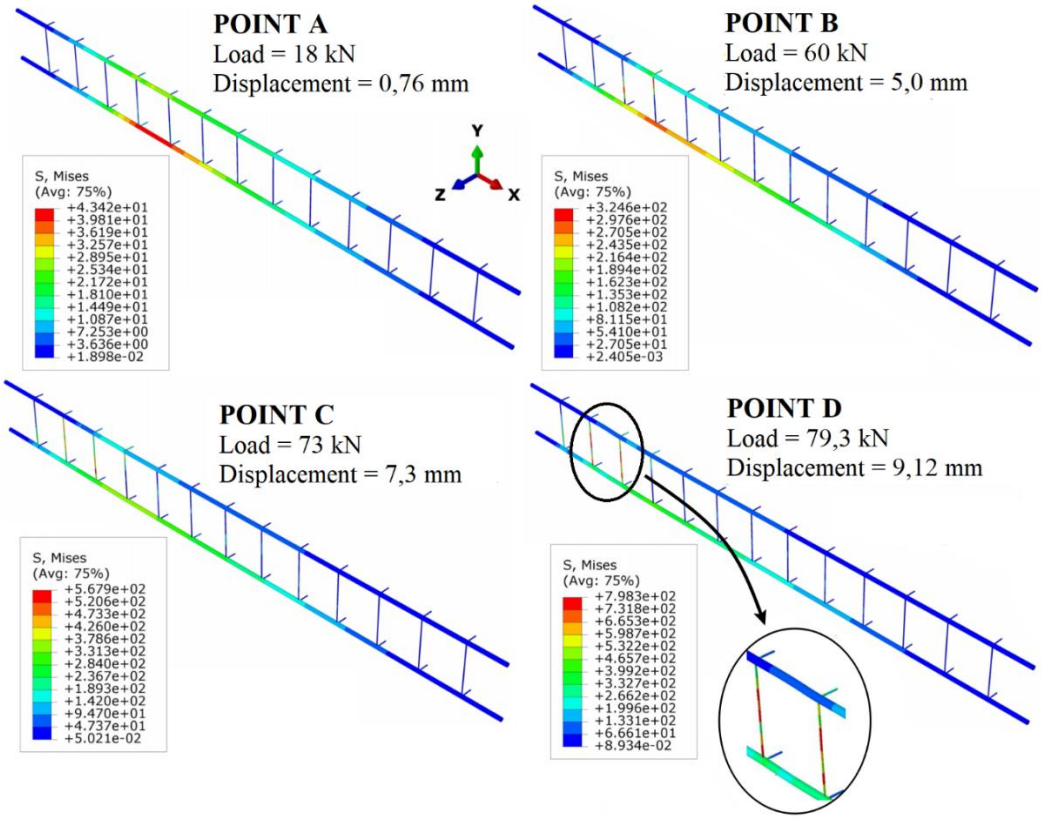


**Fig. 11.**Von Misesstressof the steel.

Fig. 12 illustrates the development of compression stresses. Up to point A, the beam behaves as a linear elastic structure, with the upper part being subject to compression and the lower part to traction. At this point, starts the compression diagonal formation. Jumaa and Yousif [41]remarked that this action begins from vertical bending tensions that propagate at an inclined angle towards the load point. With the loading process, the compressive stresses in the shear span develop completely, as in C, D, and Post – peak points.

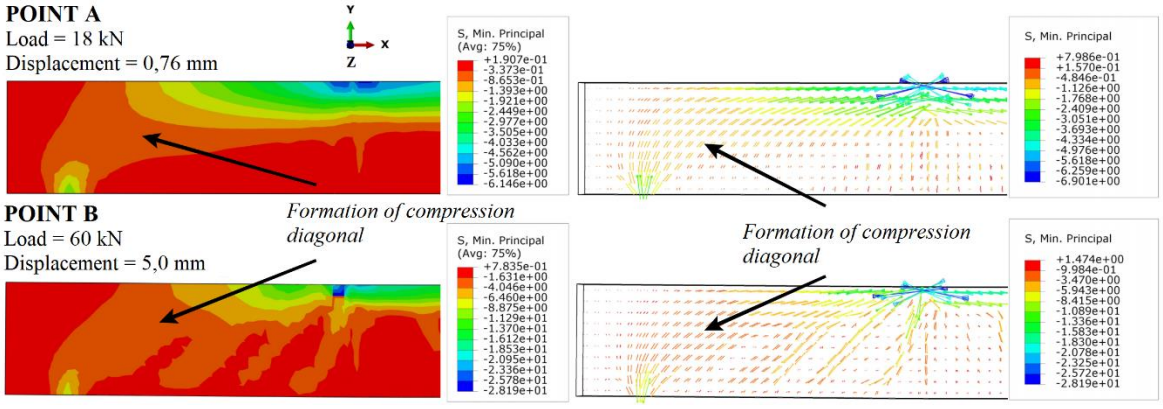

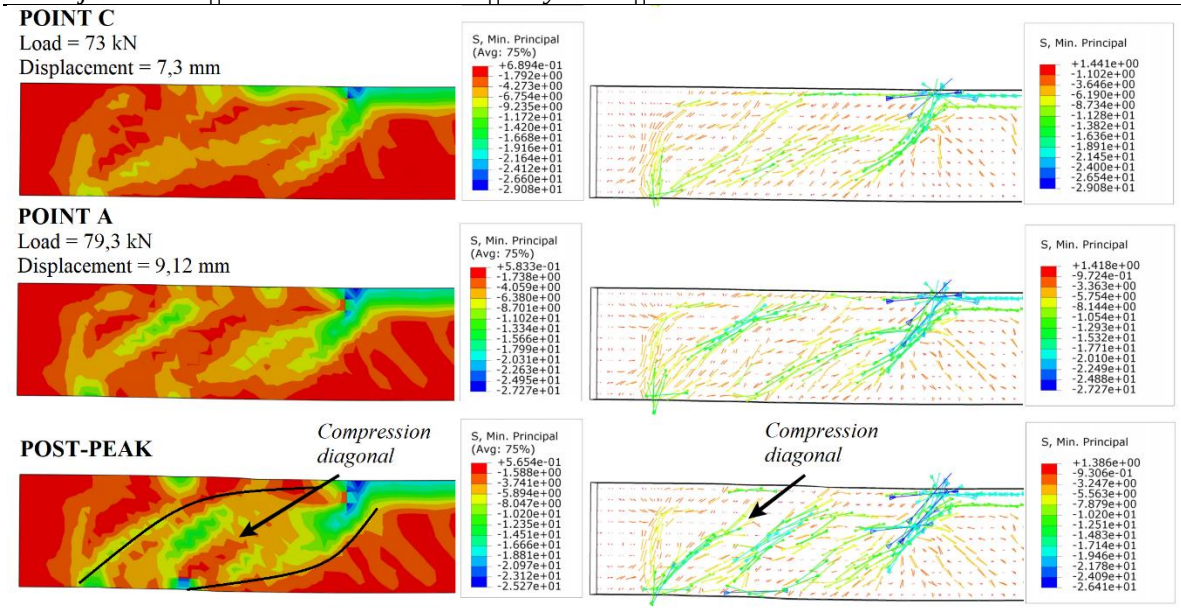


**Fig. 12.** Development of the main compression tension forces ($S_{min,principal}$) in the V0-E beam.

After calibration of the V0-E beam, its stirrups were removed as in Fig. 9 and such structure was again simulated. The test in question was named V1-S and has a load x displacement behavior represented by Fig. 13.

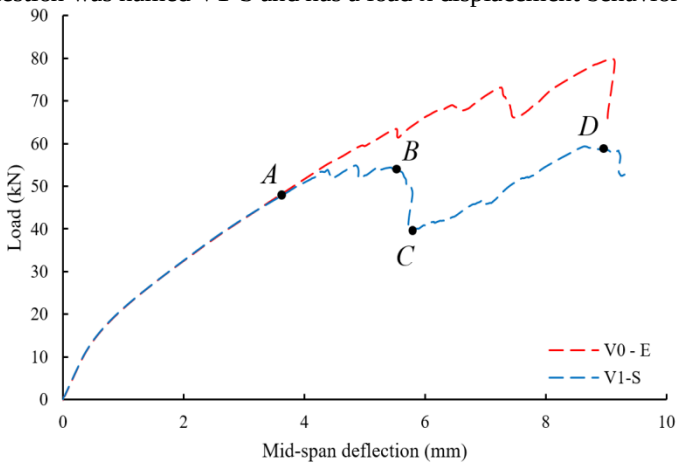


**Fig. 13.** Load x displacement chart at the middle of the span for the V1-S beam.

If we compare the graphic behavior of the V1-S simulation for the V0-E beam up to point A, the rigidity and global behavior of the structure were the same. At this moment, only bending cracks are observed, as shown in Fig. 14. At point B, the first shear cracks start to appear, resulting from the damages that resulted from bending. It is noted that due to the lack of stirrups, the crack kinematics is more concentrated than in the V0-E beam. In the latter, the diagonal fissure can still be observed, but in a band with several diagonal fissures in the shear span, besides those due to the bending. This situation has already been raised and verified experimentally by Pellegrino and Modena [42].

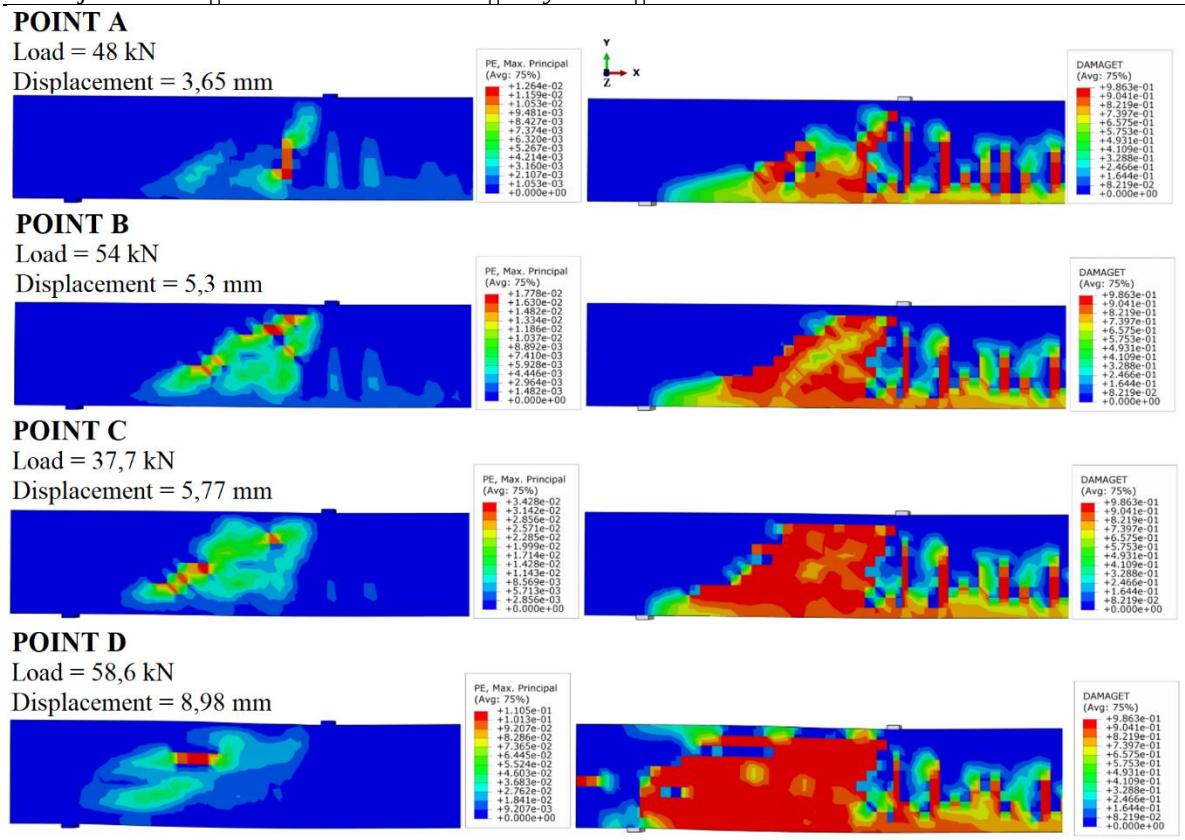


(a) (b)

**Fig. 14.**Evolution of the cracks (a) and damage to traction (b) in the V1-S beam.

## IV. CONCLUSION

The present study is a contribution to the verification of the behavior of rectangular beams in reinforced concrete subject to shear stress. The work was developed through numerical simulations using the ABAQUS [7]software, based on experimental studies. Computational models were used for the calibration: CDP for concrete, perfect elastoplastic model and bond-slip for steel.

The V0-E beam was calibrated based on the experimental beam made by Menon[27]. The dependence of the CDP parameters for good results was evident, with emphasis on the viscosity and on the angle of dilation. The increase in viscosity made the simulations faster. In contrast, the concrete presented unreal characteristics and with its increase, the load capacity of the structure increased. The beam also became more rigid. The expansion angle followed a similar pattern, since as the value of this parameter increased the beam presented higher loading capacities, but with shorter simulation time. In the latter case, it did not affect the rigidity of the structure. Regarding the mesh variation in the model, the results showed a slight dependence on the size of this parameter, which did not considerably affect the overall response of the numerical model.

Another point to be highlighted is the stiffness of the beams when adopting the bond-slip model for the longitudinal bars. Considering the perfect adhesion between steel and concrete, the rigidity of the structure increases, that is, its global displacement decreases. Knowing this, when decreasing the elasticity modulus of the longitudinal reinforcement (considering the sliding of the bars), there was a decrease of stiffness in the Concrete / Framework component, with results closer to the experimental test.

Finally, the absence of stirrups affects the overall strength of the structure, as expected. When comparing the cracking pattern of V0-E and V1-S beams with the presence of stirrups, the higher the concentration of these structures the greater is the diffusion of the cracks. This may affect future shear strengthened, as the change in the cracking pattern may affect the adhesive interface of the material.

## V. ACKNOWLEDGEMENTS

This study was financed in part by the Coordenação de Aperfeiçoamento de Pessoal de Nivel Superior – Brasil (CAPES) – Finance Code 001.

## REFERENCES

[1]. Pedroso FL. Concreto: as origens e a evolução do material construtivo mais usado pelo homem. *Rev Concreto Construções - Inst Bras Concreto*XXXVII, 2009, 77.
[2]. Fisker J and Hagsten LG. Mechanical model for the shear capacity of R/C beams without stirrups: A proposal based on limit analysis. *Eng Struct* 115, 2016, 220–231.
[3]. Cavagnis F, Fernández Ruiz M and Muttoni A. An analysis of the shear-transfer actions in reinforced concrete members without transverse reinforcement based on refined experimental measurements. *Struct Concr*19, 2018, 49–64.
[4]. Cavagnis F, Fernández Ruiz M and Muttoni A. Shear failures in reinforced concrete members without transverse reinforcement: An analysis of the critical shear crack development on the basis of test results. *Eng Struct*103, 2015, 157–73.
[5]. Bahraq AA, Al-Osta MA, Ahmad S, Al-Zahrani MM, Al-Dulaijan SO and Rahman MK. Experimental and Numerical Investigation of Shear Behavior of RC Beams Strengthened by Ultra-High Performance Concrete. *Int J Concr Struct Mater*13, 2019, 1-19.
[6]. Muttoni A and Fernández Ruiz M. From experimental evidence to mechanical modeling and design expressions: The Critical Shear Crack Theory for shear design. *Struct Concr*20, 2019, 1464–80.
[7]. Dassault Systèmes Simulia. Analysis user's guide 6.12, 2014.
[8]. Kim N, Shin YS, Choi E and Kim HS. Relationships between interfacial shear stresses and moment capacities of RC beams strengthened with various types of FRP sheets. *Constr Build Mater*93, 2015, 1170–9.
[9]. Hanif MU, Ibrahim Z, Jameel M, Ghaedi K and Aslam M. A new approach to estimate damage in concrete beams using non-linearity. *Constr Build Mater*124,2016, 1081–9.
[10]. Earij A, Alfano G, Cashell K and Zhou X. Nonlinear three–dimensional finite–element modelling of reinforced–concrete beams: Computational challenges and experimental validation. *Eng Fail Anal*82, 2017, 92–115.
[11]. Arcine MF and Menon NV. Use of cohesive interface in fe simulations of prfc strengthened beams. *Rev Tecnológica* 29, 2020, 184–98.
[12]. Abed F, El Refai A and Abdalla S. Experimental and finite element investigation of the shear performance of BFRP-RC short beams. *Structures*20, 2019, 689–701.
[13]. Jumaa GB and Yousif AR. Numerical modeling of size effect in shear strength of FRP-reinforced concrete beams. *Structures* 20, 2019, 237–54.
[14]. Bencardino F and Condello A. SRG/SRP-concrete bond-slip laws for externally strengthened RC beams. *Compos Struct* 132, 2015, 804–15.
[15]. Li LZ, Wu ZL, Yu JT, Wang X, Zhang JX and Lu ZD. Numerical simulation of the shear capacity of bolted side-plated RC beams. *Eng Struct* 171, 2018, 373–84.
[16]. Lubliner J, Oliver J, Oller S and Oñate E. A plastic-damage model for concrete. *Int J Solids Struct* 25, 1989, 299–326.
[17]. Lee J and Fenves GL. Plastic-Damage Model for Cyclic Loading of Concrete Structures. *J Eng Mech*124, 1998, 892–900.
[18]. Demin W and Fukang H. Investigation for plastic damage constitutive models of the concrete material. *Procedia Eng*210, 2017, 71–8.
[19]. Chi Y, Yu M, Huang L and Xu L. Finite element modeling of steel-polypropylene hybrid fiber reinforced concrete using modified concrete damaged plasticity. *Eng Struct*148, 2017, 23–35.
[20]. Tysmans T, Wozniak M, Remy O and Vantomme J. Finite element modelling of the biaxial behaviour of high-performance fibre-reinforced cement composites (HPFRCC) using Concrete Damaged Plasticity. *Finite Elem Anal Des*100, 2015, 47–53.
[21]. Obaidat YT, Dahlblom O and Heyden S. Nonlinear FE modelling of shear behaviour in RC beam retrofitted with CFRP. *Computational Modelling of Concrete Structures* 2010, 49–56.
[22]. Dehestani M and Mousavi SS. Modified steel bar model incorporating bond-slip effects for embedded element method. *Constr Build Mater*81, 2015, 284–90.
[23]. Díaz de Terán JR and Haach VG. Equivalent stress-strain law for embedded reinforcements considering bond-slip effects. *Eng Struct* 165, 2018, 247–53.
[24]. Belarbi A and Hsu T. Constitutive laws of concrete in tension and reinforcing bars stiffened by concrete. *ACI Struct J* 91, 1994.
[25]. Kwak HG and Kim JK. Implementation of bond-slip effect in analyses of RC frames under cyclic loads using layered section method. *Eng Struct*28, 2006, 1715–27.
[26]. Wu YF and Zhao XM. Unified bond stress-slip model for reinforced concrete. *J Struct Eng (United*

*States)*139, 2013, 1951–62.
[27]. NV Menon. *Estudo experimental de sistemas de reforço ao cisalhamento em vigas de concreto armado utilizando-se polímero reforçado com fibras de carbono (PRFC).*Doctoral dissertation, Santa Catarina, Federal University of Santa Catarina, Florianópolis, SC, 2008.
[28]. Genikomsou AS and Polak MA. Finite element analysis of punching shear of concrete slabs using damaged plasticity model in ABAQUS. *Eng Struct* 98, 2015, 38–48.
[29]. Najafgholipour MA, Dehghan SM, Dooshabi A and Niroomandi A. Finite element analysis of reinforced concrete beam-column connections with governing joint shear failure mode. *Lat Am J Solids Struct*14, 2017, 1200–25.
[30]. Al-Osta MA, Isa MN, Baluch MH and Rahman MK. Flexural behavior of reinforced concrete beams strengthened with ultra-high performance fiber reinforced concrete. *Constr Build Mater*134, 2017, 279–96.
[31]. Li C, Hao H and Bi K. Numerical study on the seismic performance of precast segmental concrete columns under cyclic loading. *Eng Struct* 2017;148:373–86.
[32]. Behnam H, Kuang JS and Samali B. Parametric finite element analysis of RC wide beam-column connections. *Comput Struct* 205, 2018, 28–44.
[33]. Gao L, Zhang F, Liu J, Lu X and Gao H. Experimental and numerical study on the interfacial bonding characteristics of FRP-to-concrete joints with mechanical fastening. *Constr Build Mater*199, 2019, 456–70.
[34]. Gao F, Tang Z, Hu B, Chen J, Zhu H and Ma J. Investigation of the interior RC beam-column joints under monotonic antisymmetrical load. *Front Struct Civ Eng*13, 2019, 1474–94.
[35]. Dabiri H, Kaviani A and Kheyroddin A. Influence of reinforcement on the performance of non-seismically detailed RC beam-column joints. *J Build Eng*31, 2020, 101333.
[36]. Carreira DJ and Chu KH. Stress-Strain Relationship for Plain Concrete in Compression. *ACI Struct J*82–72, 1986, 797–804.
[37]. Hordijk DA. Tensile and tensile fatigue behaviour of concrete; experiments, modelling and analyses. *Heron*37, 1992, 1–79.
[38]. ACI. 318-19. *Building Code Requirements for Structural Concrete and Commentary.* American Concrete Institute (ACI) Committee 440, Farmington Hills, Michigan, 2019.
[39]. Birtel V and Mark P. Parameterised Finite Element Modelling of RC Beam Shear Failure. *Abaqus User's Conf* 2006, 95–108.
[40]. Malm R. *Shear cracks in concrete structures subjected to in-plane stresses* (Trita-Bkn Bull, 2006)
[41]. Jumaa GB and Yousif AR. Size Effect in Shear Failure of High Strength Concrete Beams without Stirrup reinforced with Basalt FRP Bars. *KSCE J Civ Eng*23, 2019, 1636–50.
[42]. Pellegrino C and Modena C. Fiber Reinforced Polymer Shear Strengthening of Reinforced Concrete Beams with Transverse Steel Reinforcement. *J Compos Constr*6, 2002, 104–11.